Surface diffusion on a palladium-based metallic glass

Zijian Wang and John H. Perepezko*

Department of Materials Science and Engineering, University of Wisconsin-Madison, Madison,

Wisconsin 53706, USA

*Corresponding author: perepezko@engr.wisc.edu

Keywords: Metallic glass, surface diffusion, kinetics

Abstract

The surface diffusion kinetics on a Pd_{77.5}Cu₆Si_{16.5} metallic glass is measured using a scratch

smoothing method in the range of 107 K to 57 K below the glass transition temperature. Within

this temperature range the surface diffusion coefficients are determined to vary between (8.66 \pm

0.80) × 10^{-19} m² s⁻¹ and $(5.90 \pm 0.60) \times 10^{-18}$ m² s⁻¹. The corresponding activation energy is 0.93

 \pm 0.18 eV, which is about half the value for bulk diffusion. These measurements also corroborate

the correlation between enhanced surface diffusion and liquid fragility in glasses.

A glass is typically formed by cooling a liquid fast enough to avoid crystallization.^{1,2} The glass

inherits the disordered atomic structure of its parent liquid while maintaining a density comparable

to its crystalline counterpart.^{1,2} Glasses play a pivotal role in diverse applications ranging from

aerospace to electronics.³⁻⁵ These applications often involve important physical, chemical, or

biological processes occurring at the surfaces, such as friction, catalysis, crystallization, and thin

film formation.⁶⁻⁸ Therefore, the surface mobility on glasses, which is critical for understanding

and controlling these processes, has captured growing attention over the past few decades. 9,10

Although it has been determined that the surface of a glass exhibits enhanced dynamics compared

to the bulk, most of the research focuses on organic glasses. 11-15

First discovered in 1960, 16 metallic glasses (MGs) are among the most actively studied glass

materials. 17-20 The unique combination of nondirectional metallic bonding and noncrystalline

atomic arrangement in MGs endows them with many remarkable properties, such as high strength

and elasticity, outstanding corrosion and wear resistance, and distinctive thermoplastic

formability. 17-20 However, the multicomponent, highly active chemical nature of MGs poses a great

1

challenge for reliable surface dynamics measurements.^{21,22} Despite this challenge, there have been notable advancements in this field. For example, studies employing electron correlation microscopy uncovered a surface layer with faster dynamics on a Pt-based MG nanowire.^{23,24} The rapid coalescence of MG nanoparticles, observed by transmission electron microscopy, also revealed the enhanced surface mobility of MGs.^{25,26} Additionally, molecular dynamics simulation was applied to understand the mechanism of enhanced surface diffusion and its connections with different properties in model MGs.^{27,28} The first long-term surface dynamics measurement on MGs was presented in 2015, which quantified the enhanced surface dynamics on Pd₄₀Ni₁₀Cu₃₀P₂₀ MG using a grating decay method.²⁹ Subsequently, the surface diffusion of an Au-based MG was studied using the same method.²¹ It is worth noting that the challenge of surface contamination was addressed by in situ argon plasma cleaning within a high-vacuum furnace.²¹ However, in order to understand the enhanced surface mobility in MGs and to further make use of the insights to develop new materials through new routes and with new properties, additional MGs remain to be explored using reliable experimental techniques.

In this study, the surface diffusion coefficients of a $Pd_{77.5}Cu_6Si_{16.5}$ MG are measured at temperatures well below the glass transition temperature T_g using a scratch smoothing method. More specifically, by monitoring the changes in scratch width during annealing, the surface diffusivity at each temperature is deduced, which enables the evaluation of the activation energy for surface diffusion. Furthermore, the correlation between enhanced surface diffusion and liquid fragility is corroborated.

As one of the earliest bulk MG formers,³⁰ it has been reported that the Pd_{77.5}Cu₆Si_{16.5} alloy can be cast into a monolithic MG ingot with a diameter of up to 11 mm under moderate cooling rates.³¹ Owing to the excellent glass-forming ability, the Pd_{77.5}Cu₆Si_{16.5} alloy ribbon, prepared by melt spinning with high cooling rates of about 10^6 K s⁻¹ in this study, was confirmed to be fully amorphous by the X-ray diffraction (XRD). The MG ribbon measured about 20 μ m thick and 1 mm wide. The chemical composition of the MG ribbon was confirmed by energy-dispersive X-ray spectroscopy in a scanning electron microscope. The differential scanning calorimetry trace of the MG ribbon shows a T_g of 630 K and an onset crystallization temperature T_x of 671 K (Fig. S1 in the supplementary material), which are consistent with the values reported in literature.³²⁻³⁴ The

MG ribbon was pre-annealed at 573 K (T_g – 57 K or 0.91 T_g) for 2 hours to minimize the effects of structural relaxation.³⁵

The Pd_{77.5}Cu₆Si_{16.5} MG ribbon exhibited an atomically smooth surface. As shown by the atomic force microscopy (AFM) image (Fig. S2 in the supplementary material), the root-mean-square roughness in a 2 μm × 2 μm region can even reach 0.1 nm. This indicates that the surface is ready for nanostructure fabrication without the need for conventional time-consuming polishing steps.^{21,29} It has been demonstrated that AFM lithography is an effective technique in producing nanoscale gratings or scratches on a variety of materials due to its simplicity, low cost, and high resolution.^{36,37} This technique was employed to make scratches on the Pd_{77.5}Cu₆Si_{16.5} MG ribbon where an AFM tip coated with diamond-like carbon was moved across the surface under an applied normal force of about 4.5 μN. Further details of the scratch preparation are given in the supplementary material.

Figure 1a shows the cross-sectional profile of a typical surface scratch made on the MG ribbon and its corresponding AFM image. The scratch is asymmetric due to the uneven heights of the ridges on either side of the groove. The asymmetry is characterized by the ratio $\Delta h/d$, where Δh is the height difference and d is the depth of the scratch relative to the unscratched surface.³⁸ Based on the earlier work of King and Mullins,³⁹ Gruber and Mullins proposed that the smoothing of an asymmetric scratch during annealing can be considered in terms of an equivalent symmetric scratch.³⁸ When surface diffusion is the governing mechanism, the smoothing behavior can be described by the following equation:^{38,39}

$$w = Cw' = 6.907[B(t + t_0)]^{1/4}$$
 Eq. (1)

where w is the width of the equivalent symmetric scratch, w' is the experimentally measured width of the asymmetric scratch, C = w/w' is the correction factor dictated by the ratio $\Delta h/d$ (Fig. 1b), t is the annealing time, t_0 is a period that describes the initial state of the scratch, and B is the damping factor. This factor is defined by

$$B = D_{\rm s} \gamma \Omega^2 v / kT$$
 Eq. (2)

where D_s is the surface self-diffusion coefficient, γ is the surface tension, ν is the surface density of atoms, Ω is the atomic volume, k is the Boltzmann constant, and T is the annealing temperature. The temperature-dependent γ of a compositionally close Pd₇₆Cu₆Si₁₈ alloy was used in the

calculation of D_s .⁴⁰ It should also be pointed out that the largest $\Delta h/d$ value in this study is about 0.46, which corresponds to a C value of about 0.98 (Fig. 1b).

It is important to remove all contaminants and oxides on the surface so as to probe into the intrinsic surface dynamics of the MG ribbon. ^{21,22} To this end, before proceeding with annealing in a high-vacuum furnace at elevated temperatures, the MG ribbon was subjected to in situ argon plasma cleaning in a system modified from the one used in our previous study of the Au-based MG. ²¹ The cleaning condition was examined in an X-ray photoelectron spectrometer to determine the chemical effects of this surface treatment. The X-ray photoelectron spectrometry (XPS) depth profile shows that the ribbon can restore its nominal composition after etching out the top 1-nm-thick surface layer that is enriched in Si but poor in Pd (Fig. S3 in the supplementary material). Therefore, a duration of 100 s for plasma cleaning, which can achieve an etching depth of approximately 5 nm, is sufficient to eliminate potential contamination and expose an intrinsic surface where all the Pd, Cu and Si species are in their pure elemental state, as confirmed by the high-resolution Pd 3d, Cu 2p and Si 2p XPS spectra (Fig. S4 in the supplementary material).

Annealing of the MG ribbon was carried out at 573 K, which is 57 K below $T_{\rm g}$ or $0.91T_{\rm g}$. As shown by the XRD patterns (Fig. S5 in the supplementary material), the ribbon maintained an amorphous structure during annealing before slight crystallization was detected after 220200 s. This low annealing temperature inhibited surface crystallization from interfering too early, thereby enabling adequate observation of scratch smoothing on the MG surface. The AFM images of the scratch annealed for different times and the corresponding profiles are shown in Fig. 2a and 2b, respectively. As expected, the width of the scratch increased with the annealing time. By contrast, the depth showed intriguing changes during annealing; it increased in the first 46800 s and decreased afterwards. In fact, a complex mechanical interaction can occur between the AFM tip and the MG ribbon while making a scratch. 36,37,41 As a result, every position in the surface layer around the scratch may have a slightly different stress state. Along with the widening of the scratch, this potential difference could drive the surface layer to be more structurally homogenous. In addition, Gruber and Mullins pointed out that the use of widths rather than depths is favored in the analysis of asymmetric scratch smoothing as the former is much simpler and the latter can have

larger errors.³⁸ Therefore, the analysis of scratch smoothing focused on variations in the width of a scratch.

Previous studies imply that surface diffusion is the dominant mechanism for surface smoothing of MGs when annealed at temperatures below $0.95T_{\rm g}$. 21,24,27,29 For example, it was identified that surface diffusion governs surface smoothing on the Pd₄₀Ni₁₀Cu₃₀P₂₀ MG at 519 K, which is 47 K below its $T_{\rm g}$ or $0.92T_{\rm g}$. Similarly, surface diffusion was also determined to be responsible for the grating decay on the Au-based MG at 338 K, which is 20 K below its $T_{\rm g}$ or $0.94T_{\rm g}$. On the other hand, if volume diffusion is assigned to interpret the scratch widening at 573 K (0.91 $T_{\rm g}$), not only is the fitting quality suboptimal, but also the calculated volume diffusion coefficient $D_{\rm v}$ deviates from the experimental value significantly (Fig. S6 in the supplementary material). Therefore, it is reasonable to apply Eq. (1) to fit the data in Fig. 2c where w^4 is plotted against t. Linear fitting of the data yields a high coefficient of determination ($R^2 = 0.9699$) and a slope of 2100 \pm 200 nm⁴ s⁻¹. Based on Eq. (2), the $D_{\rm s}$ at this temperature was calculated to be $(5.90 \pm 0.60) \times 10^{-18}$ m² s⁻¹.

The MG ribbon was also annealed at two lower temperatures, namely, 553 K ($T_{\rm g}$ – 77 K or 0.88 $T_{\rm g}$) and 523 K ($T_{\rm g}$ – 107 K or 0.83 $T_{\rm g}$). The XRD patterns indicate that the MG ribbons maintained their fully amorphous structure at these two temperatures over the investigated timescales (Fig. S7 in the supplementary material). The AFM images captured at different annealing times and the corresponding profiles are shown in Fig. S8 and S9 in the supplementary material, respectively. As discussed above, Eq. (1) was used to analyze the widening of the scratches. The high coefficients of determination (R^2 = 0.9997 for 553 K and R^2 = 0.9749 for 523 K) shown in Fig. 3a and 3b indicate that the linear fits are of excellent quality. Accordingly, the $D_{\rm s}$ values at 553 K and 523 K were calculated to be (2.36 ± 0.02) × 10⁻¹⁸ m² s⁻¹ and (8.66 ± 0.80) × 10⁻¹⁹ m² s⁻¹, respectively.

Based on the Arrhenius temperature dependence of diffusivity $D_s = D_0 \exp(-E_s/kT)$, ⁴³ the activation energy for surface diffusion (E_s) can be evaluated from the linear relationship between $\ln D_s$ and 1000/T shown in Fig. 3c. The average E_s in this temperature range was determined to be 0.93 ± 0.18 eV. It is close to the E_s (0.97 eV) of the supercooled $Pd_{81}Si_{19}$ liquid that was derived from the rapid coalescence of amorphous nanoparticles.²³ In comparison, the activation energies were

evaluated to be approximately 1.67 eV and 2.10 eV for Au tracer diffusion in the same MG and in the Pd₇₈Cu₆Si₁₆ MG with an almost identical composition, respectively.^{42,44} This comparison supports the finding that the activation energy for diffusion near a free surface is about half that for bulk diffusion.⁴⁵ Figure 3c shows that by extrapolating this linear fit to higher temperatures, the D_s of the Pd_{77.5}Cu₆Si_{16.5} MG at T_g is about 2.60 × 10⁻¹⁷ m² s⁻¹.

It has been discovered that surface diffusion and its enhancement relative to bulk diffusion can be well correlated with liquid fragility for all types of glasses. 46 Liquid fragility describes the deviation of the temperature dependence of viscosity η from Arrhenius behavior; a stronger deviation corresponds to a more fragile system.² The higher resistance of a stronger system against thermal excitation around $T_{\rm g}$ stems from its more robust atomic structure. ⁴⁶ This characteristic can also make the system more resistant to the loss of nearest neighbors from bulk to surface, thereby leading to less enhanced surface mobility. 46 However, the correlation between surface diffusion enhancement (D_s/D_v) at T_g and the most widely used fragility parameter m, defined as the slope of $\log \eta$ dependence on T_g/T near T_g , 47 has not been presented yet. Here in Fig. 3d, D_s/D_v at T_g is plotted against m for the Pd_{77.5}Cu₆Si_{16.5} MG, ^{42,48} and a few other representative glasses, including SiO₂, ⁴⁹⁻⁵¹ ortho-terphenyl (OTP), ⁵²⁻⁵⁴ tris-naphtyl benzene (TNB), ⁵⁵⁻⁵⁷ indomethacin (IMC), ⁵⁸⁻⁶⁰ and two Cu-Zr MGs. ^{28,61} The data shows a good correlation between D_s/D_v at T_g and m; stronger glasses with lower values of m exhibit less pronounced enhanced surface diffusion. This correlation not only corroborates the previous findings but also holds significant promise for broader applications. Given the availability of m for many systems and the existing correlations between m and some other properties such as glass-forming ability and Poisson's ratio, 62,63 the correlation between D_s/D_v at T_g and m could be instrumental in understanding and even predicting surface mobility and related processes, such as surface crystallization and formation of highly stable glasses with desirable properties.

In summary, the method of surface scratch smoothing was used to measure the surface diffusion coefficients of a Pd_{77.5}Cu₆Si_{16.5} MG well below $T_{\rm g}$ at 573 K, 553 K and 523 K. Specifically, the surface diffusivities at these temperatures, which vary from $(8.66 \pm 0.80) \times 10^{-19}$ m² s⁻¹ to $(5.90 \pm 0.60) \times 10^{-18}$ m² s⁻¹, were obtained by following the widening of the scratches made by AFM lithography during annealing, using the model developed by Gruber and Mullins. The activation

energy for surface diffusion on this MG was then evaluated to be 0.93 ± 0.18 eV, about half that of the bulk diffusion. The findings not only support the correlation between enhanced surface mobility and liquid fragility, but they may also help pave the way for studying surface dynamics of a wide range of metallic glasses.

Supplementary Material

See the supplementary material for a complete description of the details on the sample preparation, characterization, and measurements.

Acknowledgements

We gratefully acknowledge the support of the NSF MRSEC (DMR-1720415) for the initial experimental study and the NSF MRSEC (DMR-2309000) for support of the completion of the experimental study and the analysis of the results. We also thank Prof. Lian Yu, Prof. Mark Ediger, Prof. Izabela Szlufarska and Prof. Paul Voyles for valuable discussions.

Data Availability

The data that support the findings of this study are available within the article [and its supplementary material].

References

- P. G. Debenedetti and F. H. Stillinger, Nature **410**, 259 (2001).
- ² C. A. Angell, Science **267**, 1924 (1995).
- ³ M. Telford, Mater. Today **7**, 36 (2004).
- A. Macfarlane and G. Martin, Science 305, 1407 (2004).
- ⁵ D. L. Morse and J. W. Evenson, Int. J. Appl. Glass Sci **7**, 409 (2016).
- ⁶ L. Yu, Adv. Drug Deliv. Rev. **100**, 3 (2016).
- ⁷ A. Kapoor, R. Yang, and C. Wong, Catal. Rev. Sci. Eng. **31**, 129 (1989).
- ⁸ W. H. Wang, Prog. Mater. Sci. **106**, 100561 (2019).
- ⁹ H. K. Tian, Q. Y. Xu, H. Y. Zhang, R. D. Priestley, and B. Zuo, Appl. Phys. Rev. **9**, 011316 (2022).
- M. D. Ediger and J. A. Forrest, Macromolecules **47**, 471 (2014).
- ¹¹ Z. Fakhraai and J. A. Forrest, Science **319**, 600 (2008).
- ¹² Z. Yang, Y. Fujii, F. K. Lee, C.-H. Lam, and O. K. Tsui, Science **328**, 1676 (2010).
- Y. Chai, T. Salez, J. D. McGraw, M. Benzaquen, K. Dalnoki-Veress, E. Raphaël, and J. A. Forrest, Science **343**, 994 (2014).
- ¹⁴ W. Zhang and L. Yu, Macromolecules **49**, 731 (2016).
- Z. Hao, A. Ghanekarade, N. Zhu, K. Randazzo, D. Kawaguchi, K. Tanaka, X. Wang, D. S. Simmons,
 R. D. Priestley, and B. Zuo, Nature 596, 372 (2021).

- ¹⁶ W. Klement, R. Willens, and P. Duwez, Nature **187**, 869 (1960).
- ¹⁷ A. L. Greer, Science **267**, 1947 (1995).
- ¹⁸ A. L. Greer and E. Ma, MRS Bull. **32**, 611 (2007).
- ¹⁹ A. L. Greer, Mater. Today **12**, 14 (2009).
- ²⁰ J. Schroers, Phys. Today **66**, 32 (2013).
- ²¹ C. R. Cao, L. Yu, and J. H. Perepezko, Appl. Phys. Lett. **116**, 231601 (2020).
- ²² J. M. Blakely, Prog. Mater. Sci. **10**, 395 (1963).
- P. Zhang, J. J. Maldonis, Z. Liu, J. Schroers, and P. M. Voyles, Nat. Commun. 9, 1 (2018).
- D. Chatterjee, A. Annamareddy, J. Ketkaew, J. Schroers, D. Morgan, and P. M. Voyles, ACS nano **15**, 11309 (2021).
- ²⁵ Y. Tian, W. Jiao, P. Liu, S. Song, Z. Lu, A. Hirata, and M. Chen, Nat. Commun. **10**, 5249 (2019).
- ²⁶ C. R. Cao, K. Q. Huang, J. A. Shi, D. N. Zheng, W. H. Wang, L. Gu, and H. Y. Bai, Nat. Commun. **10**, 1966 (2019).
- A. Annamareddy, P. M. Voyles, J. Perepezko, and D. Morgan, Acta Mater. 209, 116794 (2021).
- A. Annamareddy, Y. Li, L. Yu, P. M. Voyles, and D. Morgan, J. Chem. Phys. **154** (2021).
- ²⁹ C. R. Cao, Y. M. Lu, H. Y. Bai, and W. H. Wang, Appl. Phys. Lett. **107**, 141606 (2015).
- ³⁰ H. S. Chen and D. Turnbull, Acta Metall. **17**, 1021 (1969).
- H.-Y. Ding, Y. Li, and K.-F. Yao, Chin. Phys. Lett. **27**, 126101 (2010).
- ³² B. G. Bagley and E. M. Vogel, J. Non Cryst. Solids **18**, 29 (1975).
- ³³ G. Fiore and L. Battezzati, J. Alloys Compd. **483**, 54 (2009).
- ³⁴ Y. C. Tang, G. T. Ma, N. Nollmann, G. Wilde, M. Zeng, C. H. Hu, L. Li, and C. Tang, J. Mater. Res. Technol. **17**, 2203 (2022).
- F. Faupel, W. Frank, M.-P. Macht, H. Mehrer, V. Naundorf, K. Rätzke, H. R. Schober, S. K. Sharma, and H. Teichler, Rev. Mod. Phys. **75**, 237 (2003).
- A. Notargiacomo, V. Foglietti, E. Cianci, G. Capellini, M. Adami, P. Faraci, F. Evangelisti, and C. Nicolini, Nanotechnology **10**, 458 (1999).
- ³⁷ A. A. Tseng, Small **7**, 3409 (2011).
- ³⁸ E. E. Gruber and W. W. Mullins, Acta Metall. **14**, 397 (1966).
- ³⁹ R. T. King and W. W. Mullins, Acta Metall. **10**, 601 (1962).
- I. Egry, G. Lohöfer, I. Seyhan, S. Schneider, and B. Feuerbacher, Int. J. Thermophys. **20**, 1005 (1999).
- ⁴¹ A. A. Tseng, C.-F. J. Kuo, S. Jou, S. Nishimura, and J.-i. Shirakashi, Appl. Surf. Sci. **257**, 9243 (2011).
- ⁴² H. S. Chen, L. C. Kimerling, J. M. Poate, and W. L. Brown, Appl. Phys. Lett. **32**, 461 (1978).
- ⁴³ E. G. Seebauer and C. E. Allen, Prog. Surf. Sci. **49**, 265 (1995).
- J. Bøttiger, K. Dyrbye, K. Pampus, B. Torp, and P. H. Wiene, Phys. Rev. B 37, 9951 (1988).
- ⁴⁵ J. D. Stevenson and P. G. Wolynes, J. Chem. Phys. **129**, 234514 (2008).
- 46 Y. Li, A. Annamareddy, D. Morgan, Z. Yu, B. Wang, C. Cao, J. H. Perepezko, M. D. Ediger, P. M. Voyles, and L. Yu, Phys. Rev. Lett. **128**, 075501 (2022).
- ⁴⁷ R. Böhmer and C. A. Angell, Phys. Rev. B **45**, 10091 (1992).
- ⁴⁸ G. Fiore and L. Battezzati, Adv. Eng. Mater. **9**, 509 (2007).
- G. Brebec, R. Seguin, C. Sella, J. Bevenot, and J. C. Martin, Acta Metall. 28, 327 (1980).
- ⁵⁰ E. Rössler, K.-U. Hess, and V. Novikov, J. Non Cryst. Solids **223**, 207 (1998).
- ⁵¹ A. Roder, W. Kob, and K. Binder, J. Chem. Phys. **114**, 7602 (2001).
- ⁵² R. Böhmer, K. L. Ngai, C. A. Angell, and D. J. Plazek, J. Chem. Phys. **99**, 4201 (1993).
- ⁵³ M. K. Mapes, S. F. Swallen, and M. D. Ediger, J. Phys. Chem. B **110**, 507 (2006).
- ⁵⁴ W. Zhang, C. W. Brian, and L. Yu, J. Phys. Chem. B **119**, 5071 (2015).
- ⁵⁵ R. Richert, K. Duvvuri, and L.-T. Duong, J. Chem. Phys. **118**, 1828 (2003).

- ⁵⁶ S. F. Swallen, K. Traynor, R. J. McMahon, M. D. Ediger, and T. E. Mates, J. Phys. Chem. B **113**, 4600 (2009).
- ⁵⁷ S. Ruan, W. Zhang, Y. Sun, M. D. Ediger, and L. Yu, J. Chem. Phys. **145**, 064503 (2016).
- ⁵⁸ L.-M. Wang, C. A. Angell, and R. Richert, J. Chem. Phys. **125**, 074505 (2006).
- ⁵⁹ S. F. Swallen and M. D. Ediger, Soft Matter **7**, 10339 (2011).
- L. Zhu, C. W. Brian, S. F. Swallen, P. T. Straus, M. D. Ediger, and L. Yu, Phys. Rev. Lett. **106**, 256103 (2011).
- K. Russew, L. Stojanova, S. Yankova, E. Fazakas, and L. K. Varga, J.Phys.: Conf. Ser. **144**, 012094 (2009).
- O. N. Senkov, Phys. Rev. B **76**, 104202 (2007).
- ⁶³ V. N. Novikov and A. P. Sokolov, Phys. Rev. B **74**, 064203 (2006).

Figure captions

Fig. 1 (a) Profile of a typical asymmetric scratch on the Pd_{77.5}Cu₆Si_{16.5} MG. Inset: AFM image of the scratch. Scale bars: 80 nm. (b) Asymmetry correction factor C = w/w as a function of $\Delta h/d$ for surface diffusion. This figure is adapted from Ref. ³⁸.

Fig. 2 (a) AFM images and (b) the corresponding profiles of the scratch on the Pd_{77.5}Cu₆Si_{16.5} MG during annealing at 573 K. Scale bars in (a): 80 nm. (c) Scratch widening on the Pd_{77.5}Cu₆Si_{16.5} MG during annealing at 573 K. The error bars are the standard deviation of the average width at different positions. The solid line represents the best fit to the equation $w = 6.907[B(t + t_0)]^{1/4}$.

Fig. 3 Widening of the scratches on the Pd_{77.5}Cu₆Si_{16.5} MG during annealing at (a) 553 K and (b) 523 K. The error bars are the standard deviation of the average width at different positions. The solid lines are the best fits to the equation $w = 6.907[B(t+t_0)]^{1/4}$. (c) Arrhenius plot of the measured D_s values of the Pd_{77.5}Cu₆Si_{16.5} MG at 573 K, 553 K and 523 K. The solid line represents the best fit to the equation $D_s = D_0 \exp(-E_s/kT)$. The dashed line is extrapolation of the fitted line to estimate the D_s at T_g (marked by the arrow). (d) Correlation between enhanced surface diffusion (D_s/D_v at T_g) and liquid fragility m for the Pd_{77.5}Cu₆Si_{16.5} MG,^{42,48} SiO₂,⁴⁹⁻⁵¹ OTP,⁵²⁻⁵⁴ TNB,⁵⁵⁻⁵⁷ IMC,⁵⁸⁻⁶⁰ and Cu-Zr MGs.^{28,61} The dashed line is a guide.

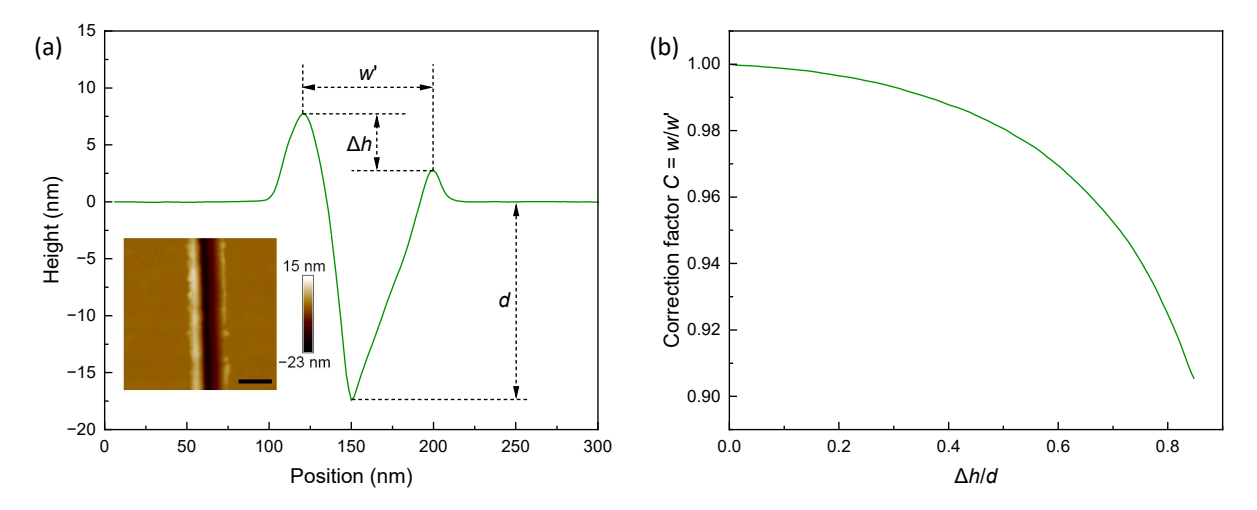


Fig. 1

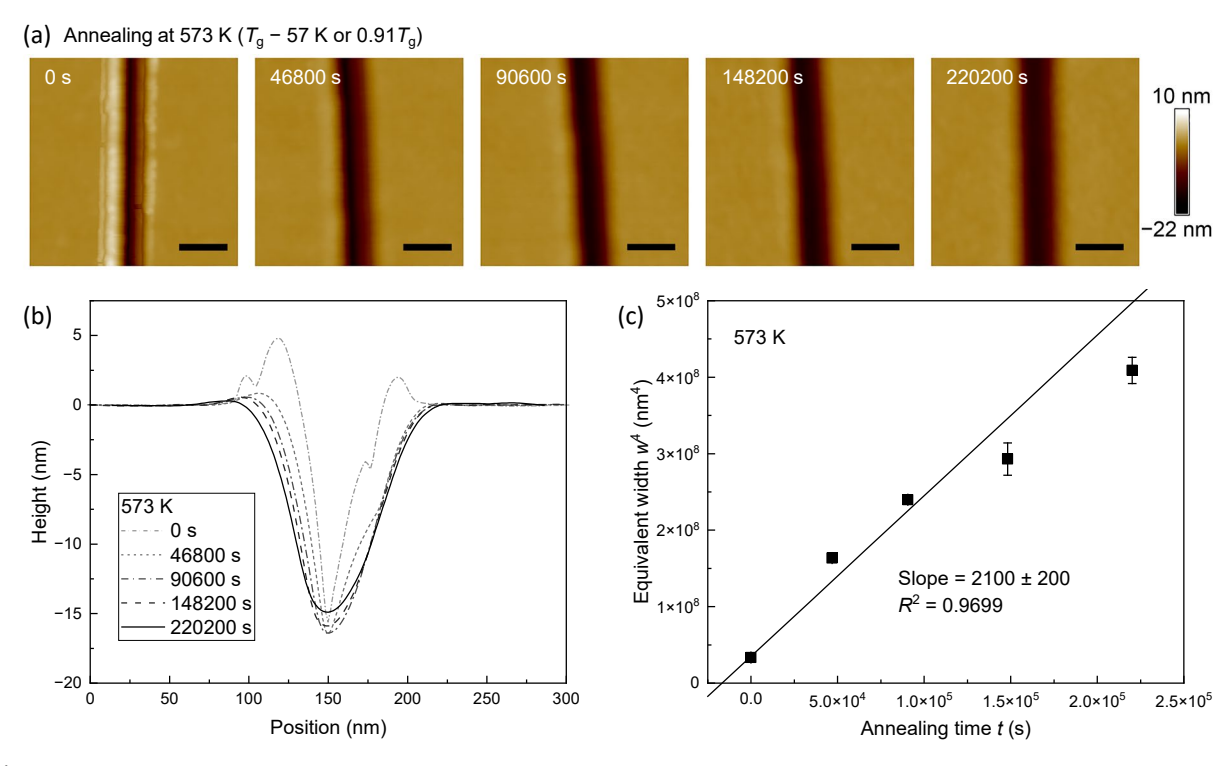


Fig. 2

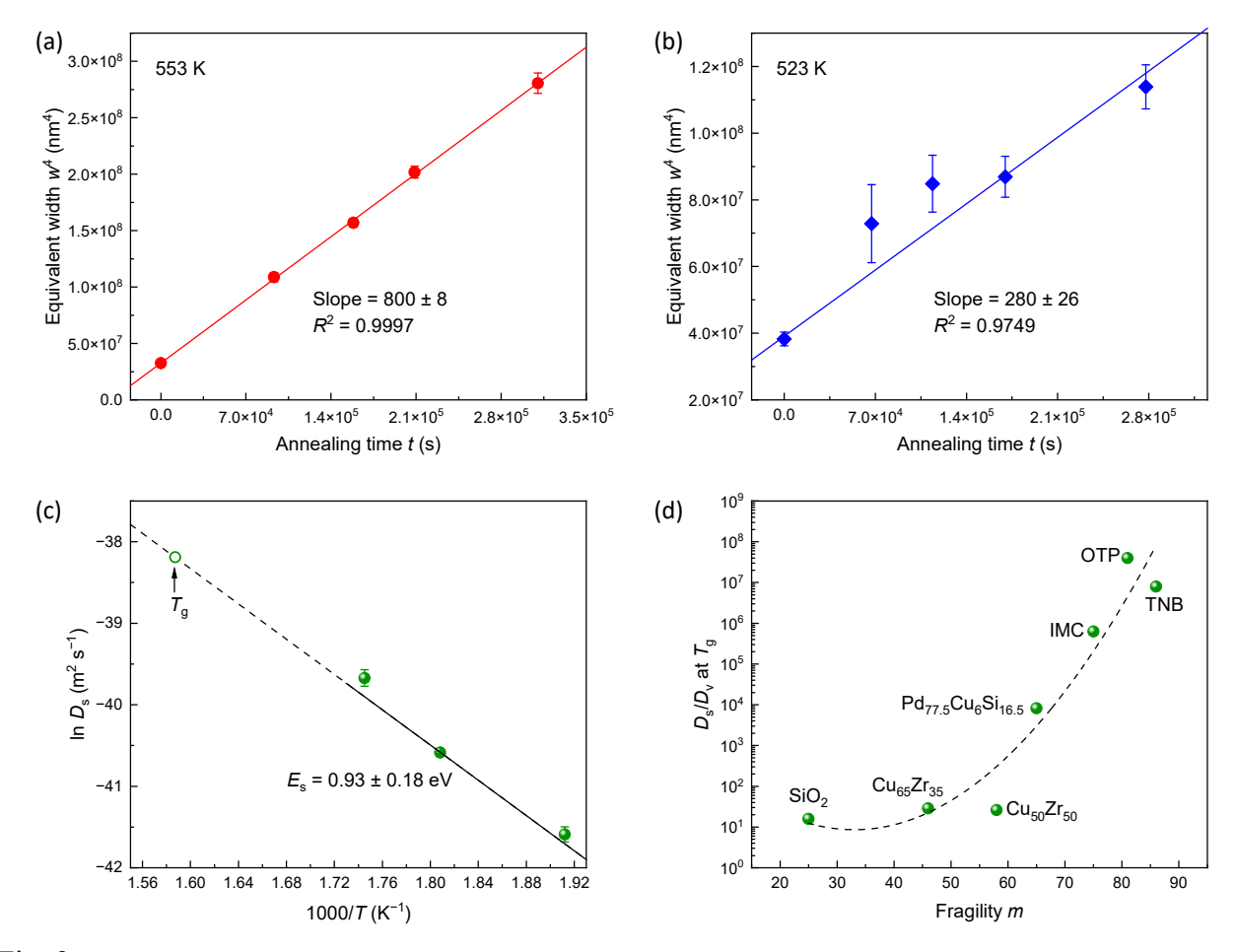


Fig. 3